International Journal of Engineering

Journal Homepage: www.ije.ir

Structural and Optical Properties of Bismuth-doped ZnO Nanoparticles Synthesized by Co-precipitation

C. Sermsrithong, P. Jaidaew, C. Promjantuk, P. Buabthong*

Physics and General Science Program, Faculty of Science and Technology, Nakhon Ratchasima Rajabhat University, Bangkok, Thailand

P A P E R   I N F O

A B S T R A C T

Bismuth-doped zinc oxide (ZnO) nanoparticles can serve as efficient photocatalysts for various reactions. Herein, we synthesized and discussed the growth mechanisms of Bi-doped ZnO nanoflakes using co-precipitation with Bi concentrations ranging from 0 to 3 %. The resulting ZnO were hexagonal nanosheets with diameters ranging from 80 nm (ZnO) to 200 nm (ZnO: Bi 3%). The dominant crystal structure matches hexagonal wurtzite with a small presence of Bi_2O_3 diffraction peaks. The estimated crystallite sizes range from ~ 33 nm to ~ 45 nm, indicating multiple crystalline regions in each nanoflake. Nevertheless, as sheet resistance monotonically decreases with the Bi concentration, the higher number of grain boundaries likely has a lower effect on the conductivity compared to an increase in free carriers and larger grain size in the samples with higher Bi concentration. The bandgap decreases from ~ 3.13 eV to ~ 2.96 eV, likely due to the shrinkage effect from electron-electron or electron-impurity interaction that lowers the conduction band of ZnO.

NOMENCLATURE

D	Crystallite size	λ	Wavelength of the X-ray
θ	Diffracting angle	β	Full-width half-max of the diffracting peak

1. INTRODUCTION

Zinc oxide (ZnO) has been one of the most versatile materials with applications ranging from optoelectronics to photocatalysis. Among different forms of ZnO, nanoparticles can provide a higher surface area, which increases the number of active sites for the reactions compared to thin films or other 2D bulk surfaces, particularly useful for catalytic applications [4]. ZnO nanoparticles have been prepared by various techniques, including sol-gel method [5], electrophoretic deposition [6], hydrothermal methods [7], thermal decomposition [8, 9], chemical vapor deposition [10], and co-precipitation [11]. Co-precipitation is considered one of the most straightforward and affordable techniques due to its minimal setup and fewer chemical precursors involved in the process; while also allowing for incorporating dopants to vary the electronic properties [12].

Since the surface area of the nanoparticles can highly influence the catalytic performance, different morphologies of the ZnO nanoparticles have been investigated, including nanorods [13], nanospheres [9], nanoplates [14], and nanowires [15]. In particular, ZnO nanosheets have been reported to exhibit better catalytic performance because of their higher number of polar facets [16, 17], which would likely be beneficial to reactions in aqueous solutions.

In addition, to further improve the photocatalytic activity of the ZnO nanoparticles, dopants are typically introduced to increase the absorption as well as potentially enhance the charge transfer on the surface. Particularly, bismuth has been used in catalytic applications, either as the cation in mixed oxide catalysts [18], or the dopant [3]. Bi dopant has been reported to

Corresponding Author Institutional Email: pakpoom.b@nrru.ac.th (P. Buabthong)

lower the bandgap of ZnO nanocatalysts [19] and accelerate the interfacial electron transfer process, thus enhancing the photocatalytic activity under UV illumination [3]. Nevertheless, the growth mechanisms of Bi-doped ZnO nanosheet using co-precipitation is still not well investigated.

Herein, we present an investigation of the structural and optical properties of Bi-doped ZnO nanoparticles using a simple co-precipitation technique. Specifically, the procedure was optimized to produce hexagonal ZnO nanosheets. We also further discuss the formation mechanisms of these particles as well as the possible factors affecting the optoelectronic properties of the ZnO samples.

2. MATERIALS AND METHODS

All chemicals were used as received, including zinc acetate hydrate ($Zn(CH_3COO)_2 \cdot 2H_2O$, AR Grade), bismuth nitrate pentahydrate ($BiN_3O_9 \cdot 5H_2O$, AR Grade), sodium hydroxide (NaOH, AR Grade), ethanol (C_2H_6O). Deionized water with a resistivity $\rho > 18$ MΩ·cm was used for the dilution processes. The zinc precursors were prepared using 0.5M of zinc acetate hydrate. For the dopant, bismuth nitrate pentahydrate was introduced to the zinc solution ranging from 0 to 3 wt% weighed using a high-precision digital scale with a sensitivity of 0.001 g, then rigorously mixed at room temperature for 15 min.

To initiate the co-precipitation process, 2.5M NaOH was gradually dropped into the zinc-bismuth solution while continuously stirring until the mixture reached pH = 13. The pH was monitored using a pH meter with a sensitivity of pH = 0.01, and the value was allowed to stabilize for 30 s after each NaOH addition. The solution was kept stirred for 15 min at room temperature. The precipitate was rigorously rinsed with DI water, vacuum dried, and rinsed again with ethanol before annealed at 80℃ for 8 hours, then heated at 550℃ for 2 hours to form zinc oxide nanoparticles.

The samples were then characterized for their optical and structural properties. Scanning electron micrographs (SEMs) were obtained with a Carl Zeiss AURIGA at an accelerating voltage of 3.00 kV with a working distance of 7.5 mm. X-ray Diffractometry (XRD) was performed using Bruker D2 Phaser with a Cu Kα monochromator with an x-ray wavelength of 1.54060 Å using 2θ angles ranging from 10º to 90º. UV-Vis spectrometer was utilized to obtain the absorption spectra at the wavelength ranging from 200 nm to 1000 nm.

For sheet resistance measurement, the nanoparticles were screen painted onto 1x1 cm glass slides and were characterized using Jandel RM3-AR four-point probe with an operating current of 10 mA.

3. RESULTS AND DISCUSSION

As-synthesized ZnO nanoparticles were first inspected for surface morphology. Figures 1(a)-1(f) show the SEM images of ZnO samples with bismuth concentration of (a) 0 %, (b) 1 %, (c) 1.5 %, (d) 2 %, (e) 2.5 % and (f) 3 %. In all concentrations, the ZnO nanoparticles were formed into hexagonal nanoflakes, showing higher contrast, and sharper morphology as the bismuth concentration increased, with the average flake diameter ranging from 80 nm (ZnO) to 200 nm (ZnO: Bi 3%). The hexagonal shape of the particle is likely due to the preferred deposition along the *a*-axis of the ZnO lattice as supposed to the other common nanorod where the deposition would be preferred along the *c*-axis. Only the local structure and the facet of the particles were assumed to have any effects on the growth orientation. The transport of the precursor ion could potentially affect the growth, but were assumed to have a minimal influence in this environment. This preferential deposition along the *a*-axis can most likely be attributed to the strong local environment (pH = 13) around the initial nucleation site of the particle, where the excess OH⁻ leads to the formation of zinc hydroxide complex $Zn(OH)_4^{2-}$ from the Zn^{2+}, that was dissociated from the zinc acetate hydrate precursor. The negatively charged zinc hydroxide complex was then repelled from the negative surface of ZnO along the *c*-axis (100) orientation, thus resulting in more prominent 2D hexagonal flakes. This preferential growth on the 2D
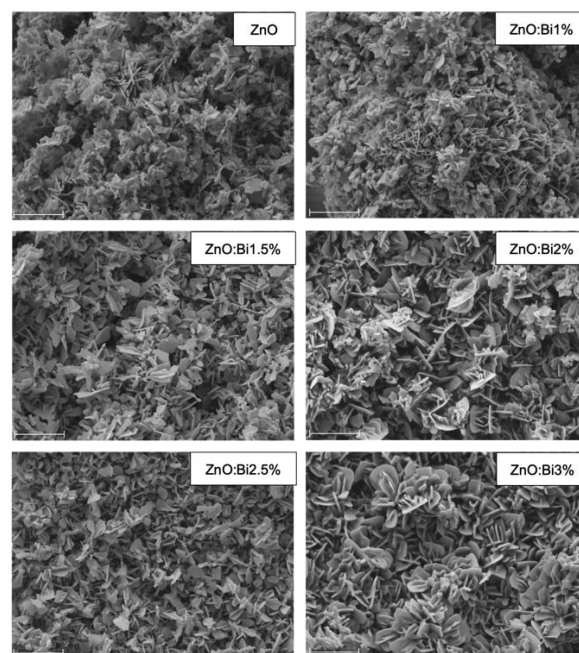

Figure 1. Scanning electron micrographs of ZnO with Bi concentration ranging from 0% to 3%, with the scalebar representing 1 µm

plane is also likely more observable in the co-precipitation technique, where the deposition mechanisms rely heavily on diffusion and adsorption of the precursors.

In addition, larger hexagonal flakes and the shaper 2D morphology were observed as higher Bi concentration was introduced. The positively charged Bi^{3+} from the bismuth nitrate precursor likely creates a more favorable local deposition environment at the ZnO sites, assisting the oxidation of the zinc hydroxide complex around the edge of the nanosheet. This preferred deposition can also be observed from having less residual deposition in other orientations in the samples with lower Bi concentration (Figure 1: ZnO and ZnO: Bi1%).

Figure 2 shows XRD patterns of the as-prepared Bi-doped ZnO nanoparticles with different Bi concentrations. The peaks at 2θ=~27.5° and ~33.2° represent the Bi_2O_3 peaks which can be observed in all samples except ZnO with no Bi dopant [20]. The main diffracting peaks were observed for the (100), (002), and (101) orientation of wurtzite ZnO at $2\theta = 31.8°$, 34.6°, and 36.4°, respectively, with the remaining peaks corresponding to the (102), (110), (103), and (112) orientation [21]. The locations of the diffraction peaks match precisely with the standards as well as the ZnO particles with different morphology and different preparation techniques [9]. The intensities of the diffraction peaks are all comparable even with increasing Bi concentration, indicating that the amount of the Bi dopant in the lattice is not sufficient to have any effect on the overall crystal structure of the ZnO host. The intensity of the (002) peak is comparable to that of (100), suggesting growth along the planar axis, [22] which is in good accord with the observed morphology (Figure 1).

Table 1 summarizes the crystallite size (D) estimated from the XRD pattern (Figure 2) using Scherrer's equation:
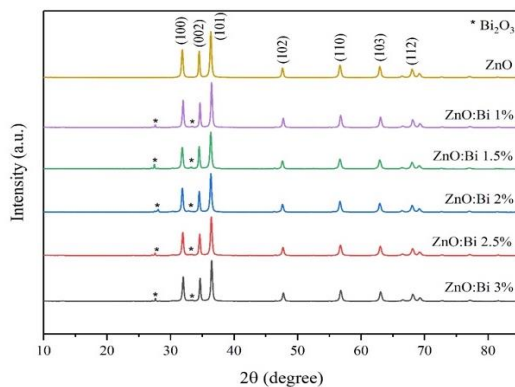
$$D = \frac{0.94\lambda}{\beta \cos\theta} \tag{1}$$

TABLE 1. Estimated crystallite size using Scherrer's equation

ZnO:Bi (%)	Crystalline size (nm)
0	33.58
1	41.79
1.5	41.95
2	42.06
2.5	42.53
3	44.65

where λ is the x-ray wavelength, β is the full-width half max (FWHM), and θ is the Bragg diffraction angle. The crystallite size monotonically increases with the Bi concentration, agreeing with more favorable deposition environment under the presence of Bi^{3+} cation. Nevertheless, the crystallite size is still substantially smaller than the size of each hexagonal nanoflake (Figure 1), suggesting that each flake may consist of multiple crystallites. Moreover, the average diameter of the flake increases by more than twice from ~ 80 nm to ~ 200 nm, while the estimated crystallite size increases from ~ 33 nm to ~ 45 nm, indicating that new nucleation sites on each nanosheet could be developed during the deposition, especially on the larger flakes and higher Bi concentration.

In addition, the distribution of the crystalline region in the sample also has a strong influence on the resistance. Since electronic conduction relies predominantly on the transport of free carriers in the sample, larger grain size typically leads to lower sheet resistance, while grain boundaries between multiple crystallites usually increase the sheet resistance. Figure 3 shows the sheet resistance of the ZnO nanoparticles with different Bi concentrations. The measured resistance monotonically decreases from ~ 58 Ω sq^{-1} in an undoped ZnO to ~ 20 Ω sq^{-1} in the 3%-doped ZnO. The reduction in sheet resistance with higher Bi concentration is likely

Figure 2. X-ray diffractometry patterns of Bi-doped ZnO with Bi concentration 0% to 3%
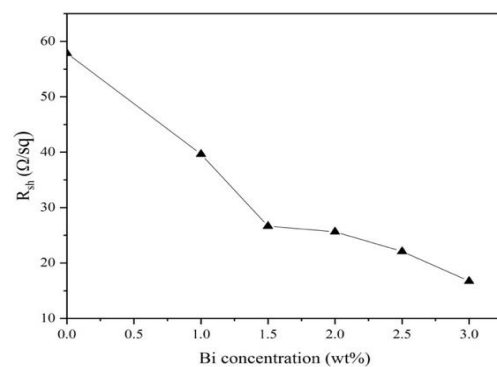

Figure 3. Sheet resistance of the ZnO nanoparticles as a function of Bi concentrations

due to an increase in free electrons from Bi^{3+} donors in the lattice. Although the conductivity was previously reported to decrease at specific Bi concentrations because of the segregation of Bi atoms at the grain boundaries [23], the monotonic decrease in the observed resistance suggests that the Bi concentration used in this experiment is still low or the grain boundary resistance is negligible at this scale.

The absorbance of the nanoparticles was measured with the wavelength sweeping from 350 nm to 800 nm, shown in Figure 4, which gradually increases and peaks at ~ 370 nm for all samples, then slowly decreases to the baseline. Similar peak positions at ~ 370 nm have also been observed in other study as the hexagonal wurtzite phase [24]. These absorbance spectra were then used to calculate the bandgap of the ZnO samples with Tauc relation [25]:

$$\alpha h\nu = E(h\nu - E_g)^{\frac{1}{2}} \qquad (2)$$

where α is the optical absorption coefficient from Figure 4, $h\nu$ is the photon energy, E_g is the bandgap, E is a fitting constant, and the power of $\frac{1}{2}$ indicating direct bandgap transition of ZnO. Figure 5(a) shows the example Tauc plot using the absorption from the undoped ZnO sample, with the straight line extrapolated from the right regime of the curve and the x-intercept of this line representing the derived bandgap of the material. Figure5(b) shows the calculated bandgap with varying Bi
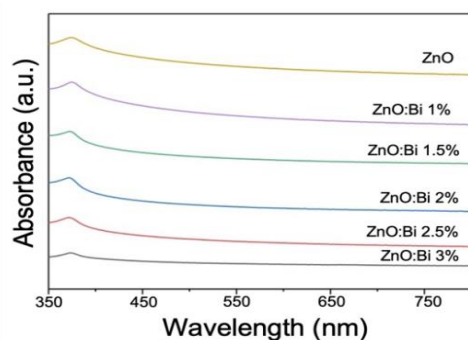

Figure 4. Absorbance of the ZnO nanoparticles as a function of wavelength
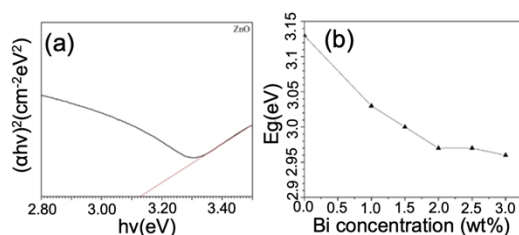

Figure 5. (a) Tauc plot of ZnO nanoparticles and (b) Bandgap of the ZnO nanoparticles as a function of Bi concentrations

concentration, where the bandgap decreases sharply from 0 % to 2 %, then remains relatively constant between 2 % to 3 %. The decrease can primarily be attributed to the shrinkage effect, which results in a lowering of the conduction band due to the net attractive interaction between electron-electron and electron-impurity interaction. Nevertheless, the more minor change after 2% dopant is likely due to fluctuation that comes from both the broadening of the valence band as well as the lowering of the conduction band [26–28].

4. CONCLUSIONS

Bi-doped ZnO nanoparticles were successfully prepared using co-precipitation using minimal laboratory setup. The morphology of the nanoparticles reveals that hexagonal nanosheets were produced, mostly by maintaining high alkalinity of the solution, with the average diameter increasing from 80 nm to 200 nm with higher Bi concentration. The wurtzite structure was observed, with the average crystallite size ranging from ~ 33 nm to ~ 45 nm, suggesting multiple crystalline regions in each nanoflake. Nevertheless, grain boundary resistance likely has minimal effect on the conductivity of the free carriers in these particles, as the sheet resistance decreases monotonically with the dopant concentration. The decrease in the optical bandgap with higher Bi concentration is likely due to the shrinkage effect from the electron-electron and electron-impurity interaction that leads to the lowered conduction band. However, the decrease of the bandgap gradually diminishes as the Bi concentration is > 2 %. These results show co-precipitation as a viable technique to synthesize Bi-doped ZnO nanosheets that exhibit optoelectronic and structural properties similar to those prepared using more sophisticated techniques. Nevertheless, further precise optimization of the electronic properties such fine-tuning the absolute band edge positions might require a more advance technique such as chemical vapor deposition.

5. ACKNOWLEDGMENT

6. REFERENCES

1.   Lokhande, B. J., and Uplane, M. D. "Structural, optical and electrical studies on spray deposited highly oriented ZnO films." *Applied Surface Science*, Vol. 167, No. 3-4, (2000), 243-246. https://doi.org/10.1016/S0169-4332(00)00533-X

2. Kang, Y., Yu, F., Zhang, L., Wang, W., Chen, L., and Li, Y. "Review of ZnO-based nanomaterials in gas sensors." *Solid State Ionics*, Vol. 360, (2021), 115544. https://doi.org/10.1016/j.ssi.2020.115544

3. Chandraboss, V. L., Natanapatham, L., Karthikeyan, B., Kamalakkannan, J., Prabha, S., and Senthilvelan, S. "Effect of bismuth doping on the ZnO nanocomposite material and study of its photocatalytic activity under UV-light." *Materials Research Bulletin*, Vol. 48, No. 10, (2013), 3707-3712. https://doi.org/10.1016/j.materresbull.2013.05.121

4. Siddiqi, K. S., ur Rahman, A., Tajuddin, and Husen, A. "Properties of Zinc Oxide Nanoparticles and Their Activity Against Microbes." *Nanoscale Research Letters*, Vol. 13, No. 1, (2018), 141. https://doi.org/10.1186/s11671-018-2532-3

5. Vaezi, M. R., and Zameni, M. "Synthesis of zinc oxide nanostructured thin film by sol-gel method and evaluation of gas sensing properties." *International Journal of Engineering, Transactions B: Applications*, Vol. 27, No. 5, (2014), 757-762. https://doi.org/10.5829/idosi.ije.2014.27.05b.11

6. Lommens, P., van Thourhout, D., Smet, P. F., Poelman, D., and Hens, Z. "Electrophoretic deposition of ZnO nanoparticles, from micropatterns to substrate coverage" *Nanotechnology*, Vol. 19, No. 24, (2008), 245301. https://doi.org/10.1088/0957-4484/19/24/245301

7. Bulcha, B., Leta Tesfaye, J., Anatol, D., Shanmugam, R., Dwarampudi, L. P., Nagaprasad, N., Bhargavi, V. L. N., and Krishnaraj, R. "Synthesis of Zinc Oxide Nanoparticles by Hydrothermal Methods and Spectroscopic Investigation of Ultraviolet Radiation Protective Properties." *Journal of Nanomaterials*, Vol. 2021, (2021), 1-10. https://doi.org/10.1155/2021/8617290

8. Hajiashrafi, S., and Motakef Kazemi, N. "Preparation and evaluation of ZnO nanoparticles by thermal decomposition of MOF-5." *Heliyon*, Vol. 5, No. 9, (2019), e02152. https://doi.org/10.1016/j.heliyon.2019.e02152

9. Darezereshki, E., Vakylabad, A. B., and Yousefi, M. "Chemical process of synthesizing zinc oxide (ZnO) with nanorod and spherical morphologies." *International Journal of Engineering, Transactions B: Applications*, Vol. 34, No. 8, (2021), 1888-1897. https://doi.org/10.5829/ije.2021.34.08b.10

10. Reuge, N., Bacsa, R., Serp, P., and Caussat, B. "Chemical Vapor Synthesis of Zinc Oxide Nanoparticles: Experimental and Preliminary Modeling Studies." *The Journal of Physical Chemistry C*, Vol. 113, No. 46, (2009), 19845-19852. https://doi.org/10.1021/jp9070955

11. Purwaningsih, S. Y., Zainuri, M., Triwikantoro, T., Pratapa, S., and Darminto, D. "Structural, optical and defect state analyses of ZnO nanoparticle films." *International Journal of Engineering, Transactions B: Applications*, Vol. 33, No. 5, (2020), 852-860. https://doi.org/10.5829/IJE.2020.33.05B.17

12. Priscilla, S. J., Judi, V. A., Daniel, R., and Sivaji, K. "Effects of Chromium Doping on the Electrical Properties of ZnO Nanoparticles." *Emerging Science Journal*, Vol. 4, No. 2, (2020), 82-88. https://doi.org/10.28991/esj-2020-01212

13. Wang, T. X., and Lou, T. J. "Solvothermal synthesis and photoluminescence properties of ZnO nanorods and nanorod assemblies from ZnO_2 nanoparticles." *Materials Letters*, Vol. 62, No. 15, (2008), 2329-2331. https://doi.org/10.1016/j.matlet.2007.11.083

14. Jang, J. S., Yu, C.-J., Choi, S. H., Ji, S. M., Kim, E. S., and Lee, J. S. "Topotactic synthesis of mesoporous ZnS and ZnO nanoplates and their photocatalytic activity." *Journal of Catalysis*, Vol. 254, No. 1, (2008), 144-155. https://doi.org/10.1016/j.jcat.2007.12.010

15. Ding, Y., and Wang, Z. L. "Structures of planar defects in ZnO nanobelts and nanowires." *Micron*, Vol. 40, No. 3, (2009), 335-342. https://doi.org/10.1016/j.micron.2008.10.008

16. Hsu, Y.-K., Lin, Y.-G., and Chen, Y.-C. "Polarity-dependent photoelectrochemical activity in ZnO nanostructures for solar water splitting." *Electrochemistry Communications*, Vol. 13, No. 12, (2011), 1383-1386. https://doi.org/10.1016/j.elecom.2011.08.016

17. Sun, J., Cao, J., and Jiang, X. "Preparation and photoelectric properties of Bi doped ZnO nanoarrays." *Journal of Alloys and Compounds*, Vol. 896, (2022), 162801. https://doi.org/10.1016/j.jallcom.2021.162801

18. Araujo Scharnberg, A. R., Carvalho de Loreto, A., and Kopp Alves, A. "Optical and Structural Characterization of Bi2FexNbO7 Nanoparticles for Environmental Applications." *Emerging Science Journal*, Vol. 4, No. 1, (2020), 11-17. https://doi.org/10.28991/esj-2020-01205

19. Singh, B. K., and Tripathi, S. "Influence of Bi concentration on structural and optical properties of Bi doped p-type ZnO thin films prepared by sol-gel method." *Journal of Materials Science: Materials in Electronics*, Vol. 27, No. 3, (2016), 2360-2366. https://doi.org/10.1007/s10854-015-4033-9

20. Oudghiri-Hassani, H., Rakass, S., al Wadaani, F. T., Al-ghamdi, K. J., Omer, A., Messali, M., and Abboudi, M. "Synthesis, characterization and photocatalytic activity of α-Bi_2O_3 nanoparticles." *Journal of Taibah University for Science*, Vol. 9, No. 4, (2015), 508-512. https://doi.org/10.1016/j.jtusci.2015.01.009

21. Arefi, M. R., and Rezaei-Zarchi, S. "Synthesis of Zinc Oxide Nanoparticles and Their Effect on the Compressive Strength and Setting Time of Self-Compacted Concrete Paste as Cementitious Composites." *International Journal of Molecular Sciences*, Vol. 13, No. 4, (2012), 4340-4350. https://doi.org/10.3390/ijms13044340

22. Ebrahimifard, R., Abdizadeh, H., and Golobostanfard, M. R. "Controlling the extremely preferred orientation texturing of sol-gel derived ZnO thin films with sol and heat treatment parameters." *Journal of Sol-Gel Science and Technology*, Vol. 93, No. 1, (2020), 28-35. https://doi.org/10.1007/s10971-019-05157-2

23. Chouikh, F., Beggah, Y., and Aida, M. S. "Optical and electrical properties of Bi doped ZnO thin films deposited by ultrasonic spray pyrolysis." *Journal of Materials Science: Materials in Electronics*, Vol. 22, No. 5, (2011), 499-505. https://doi.org/10.1007/s10854-010-0167-y

24. Wahab, R., Ansari, S. G., Kim, Y. S., Song, M., and Shin, H.-S. "The role of pH variation on the growth of zinc oxide nanostructures." *Applied Surface Science*, Vol. 255, No. 9, (2009), 4891-4896. https://doi.org/10.1016/j.apsusc.2008.12.037

25. Makuła, P., Pacia, M., and Macyk, W. "How To Correctly Determine the Band Gap Energy of Modified Semiconductor Photocatalysts Based on UV-Vis Spectra." *The Journal of Physical Chemistry Letters*, Vol. 9, No. 23, (2018), 6814-6817. https://doi.org/10.1021/acs.jpclett.8b02892

26. Auvergne, D., Camassel, J., and Mathieu, H. "Band-gap shrinkage of semiconductors." *Physical Review B*, Vol. 11, No. 6, (1975), 2251-2259. https://doi.org/10.1103/PhysRevB.11.2251

27. Yildiz, A., Ozturk, E., Atilgan, A., Sbeta, M., Atli, A., and Serin, T. "An Understanding of the Band Gap Shrinkage in Sn-Doped ZnO for Dye-Sensitized Solar Cells." *Journal of Electronic Materials*, Vol. 46, No. 12, (2017), 6739-6744. https://doi.org/10.1007/s11664-017-5778-0

28. Keskenler, E. F., Aydın, S., Turgut, G., and Doğan, S. "Optical and Structural Properties of Bismuth Doped ZnO Thin Films by Sol-Gel Method: Urbach Rule as a Function of Crystal Defects." *Acta Physica Polonica A*, Vol. 126, No. 3, (2014), 782-787. https://doi.org/10.12693/APhysPolA.126.782

Persian Abstract

چکیده

نانوذرات اکسید روی دوپ شده با بیسموت (ZnO)می توانند به عنوان فوتوکاتالیست کارآمد برای واکنش های مختلف عمل کنند. در اینجا، ما مکانیسم‌های رشد نانوفلکه‌های اکسید روی دوپه‌شده را با استفاده از رسوب همزمان با غلظت‌های بی از ۰ تا ۳ درصد ستتز و مورد بحث قرار دادیم. ZnO حاصل، نانوصفحات شش ضلعی با قطرهای ۸۰ نانومتر (ZnO)تا ۲۰۰ نانومتر (ZnO: Bi 3%)بود. ساختار کریستالی غالب با ورتزیت شش ضلعی با حضور کمی از قله های پراش Bi₂O₃ مطابقت دارد. اندازه کریستالیت تخمین زده شده از ۳۳ نانومتر تا ٤٥ نانومتر متغیر است که نشان دهنده چندین ناحیه کریستالی در هر نانوفلکه است. با این وجود، از آنجایی که مقاومت ورق به طور یکنواخت با غلظت Bi کاهش می یابد، تعداد بیشتر مرزهای دانه احتمالاً تأثیر کمتری بر هدایت در مقایسه با افزایش حامل های آزاد و اندازه دانه بزرگتر در نمونه های با غلظت Bi بالاتر دارد. فاصله باند از ~ ۳.۱۳ eV به ~ ۲.۹٦ eV کاهش می یابد، که احتمالاً به دلیل اثر انقباض ناشی از برهمکنش الکترون–الکترون یا الکترون–ناخالصی است که نوار رسانایی ZnO را کاهش می دهد.